Eur Radiol (2014) 24:3076–3087
DOI 10.1007/s00330-014-3343-2

HEAD AND NECK

Initial experience of correlating parameters of intravoxel incoherent motion and dynamic contrast-enhanced magnetic resonance imaging at 3.0 T in nasopharyngeal carcinoma

Qian-Jun Jia · Shui-Xing Zhang · Wen-Bo Chen · Long Liang · Zheng-Gen Zhou · Qian-Hui Qiu · Zai-Yi Liu · Qiong-Xin Zeng · Chang-Hong Liang

Received: 5 February 2014 / Revised: 4 June 2014 / Accepted: 11 July 2014 / Published online: 23 July 2014

Abstract
Purpose To determine the correlation between intravoxel incoherent motion (IVIM) and dynamic contrast-enhanced (DCE) magnetic resonance imaging (MRI) parameters.
Methods Thirty-eight newly diagnosed NPC patients were prospectively enrolled. Diffusion-weighted images (DWI) at 13 *b*-values were acquired using a 3.0-T MRI system. IVIM parameters including the pure molecular diffusion (*D*), perfusion-related diffusion (*D**), perfusion fraction (*f*), DCE-MRI parameters including maximum slope of increase (MSI), enhancement amplitude (EA) and enhancement ratio (*ER*) were calculated by two investigators independently. Intra- and interobserver agreement were evaluated using the intraclass correlation coefficient (*ICC*) and Bland-Altman analysis. Relationships between IVIM and DCE-MRI parameters were evaluated by calculation of Spearman's correlation coefficient.
Results Intra- and interobserver reproducibility were excellent to relatively good (ICC = 0.887-0.997; narrow width of 95 % limits of agreement). The highest correlation was observed between *f* and EA (r=0.633, P<0.001), with a strong correlation between *f* and MSI (r=0.598, P=0.001). No correlation was observed between *f* and ER (r=-0.162; P=0.421) or *D** and DCE parameters (r=0.125–0.307; P>0.119).
Conclusion This study suggests IVIM perfusion imaging using 3.0-T MRI is feasible in NPC, and *f* correlates significantly with EA and MSI.
Key Points
- *Assessment of tumour perfusion is important in nasopharyngeal carcinoma.*
- *DCE-MRI provided perfusion information with the use of intravenous contrast media.*
- *Perfusion information could be provided by non-invasive IVIM MRI.*
- *IVIM parameter f correlated with DCE-MRI parameters.*

Keywords Nasopharyngeal carcinoma · Intravoxel incoherent motion (IVIM) · Diffusion-weighted MR imaging · Dynamic contrast-enhanced MR imaging · Perfusion

Qian-Jun Jia and Shui-Xing Zhang contributed equally to this manuscript.

Q.-J. Jia · S.-X. Zhang · W.-B. Chen · L. Liang · Z.-G. Zhou · Z.-Y. Liu · Q.-X. Zeng · C.-H. Liang (✉)
Department of Radiology, Guangdong General Hospital/Guangdong Academy of Medical Sciences, 106 Zhong Shan Er Road, Guangzhou, Guangdong Province 510080, People's Republic of China
e-mail: cjr.lchh@vip.163.com

Q.-J. Jia
e-mail: jiaqianjun@126.com

S.-X. Zhang
e-mail: shui7515@126.com

W.-B. Chen
e-mail: wbchen5@163.com

L. Liang
e-mail: L_Diplodocus163@163.com

Z.-G. Zhou
e-mail: zhouzhenggen@163.com

Z.-Y. Liu
e-mail: zyliu@163.com

Q.-X. Zeng
e-mail: qxzeng_1238@126.com

Q.-H. Qiu
Department of Otolaryngology, Guangdong General Hospital/Guangdong Academy of Medical Sciences, 106 Zhong Shan Er Road, Guangzhou, Guangdong Province 510080, People's Republic of China
e-mail: qiuqianhui@hotmail.com

Abbreviations

CBV	Cerebral blood volume
D	Pure molecular diffusion
DCE	Dynamic contrast-enhanced
DWI	Diffusion-weighted images
D*	Perfusion-related diffusion
EA	Enhancement amplitude
ER	Enhancement ratio
f	Perfusion fraction
FOV	Field of view
IVIM	Intravoxel incoherent motion
ICC	Intraclass correlation coefficient
LoA	Limits of agreement
MRI	Magnetic resonance imaging
MSI	Maximum slope of increase
MVD	Microvessel density
MTT	Mean transit time
NEX	Number of excitations
NPC	Nasopharyngeal carcinoma
SPGR	Spoiled gradient-recalled echo
TR	Repetition time
TE	Echo time
TICs	Time-signal intensity curves
VEGFR-2	Vascular endothelial growth factor receptor 2

Introduction

Nasopharyngeal carcinoma (NPC) is rare throughout most of the world, but has a markedly varied geographic and racial pattern of incidence [1] and is endemic in several high-risk populations, including individuals originating from China in whom NPC accounts for 15–18 % of malignancies [2].

Assessment of local perfusion is an important component of the diagnosis and evaluation of NPC [3, 4]. Dynamic contrast-enhanced magnetic resonance imaging (DCE-MRI) has been applied in oncology for the purpose of characterising tumour perfusion. In previous studies concerning head and neck cancer including NPC, DCE-MRI was shown to be useful for distinguishing between undifferentiated carcinoma and squamous cell carcinoma or lymphoma, and it also has proven value for differentiating between recurrent tumours and post-treatment fibrotic changes [5, 6]. However, DCE-MRI cannot provide perfusion information without the use of intravenous contrast media, which is particularly relevant in patients with compromised renal function or individuals with severe allergies who cannot tolerate intravenous gadolinium-based contrast media [7].

Intravoxel incoherent motion (IVIM)-based diffusion-weighted imaging (DWI) is a non-contrast-enhanced MRI technique, which was initially developed by Le Bihan et al. [8, 9]. IVIM perfusion-related parameters include: the perfusion fraction (*f*), which describes the fraction of incoherent signal that arises from the vascular compartment in each voxel as a proportion of the total incoherent signal, and the pseudo-diffusion coefficient (*D**), which macroscopically describes the incoherent movement of blood in the microvascular compartment. Furthermore, a theoretical relationship has been derived between the IVIM perfusion parameters *f* and *D** and the classical perfusion parameters cerebral blood volume (CBV) and mean transit time (MTT) [10]. On this basis, we assumed that we could identify IVIM perfusion parameters associated with DCE-MRI parameters using DWI. If perfusion parameters could be evaluated using DWI, then DWI might potentially become a very valuable and convenient tool for the comprehensive assessment of tumours.

A number of recent reports have described the measurement of perfusion parameters using IVIM in various diseases of different organs, such as the brain [11], salivary glands [12], and head and neck cancer [13]. While initial reports of the use of IVIM have been made in different tumour stages of NPC and to compare NPC with post-chemoradiation fibrosis [14, 15], to our knowledge, no existing reports have compared the relationship between IVIM parameters and DCE-MRI perfusion parameters in primary NPC.

Therefore, the purpose of this study was to evaluate the relationship between IVIM parameters of tumour perfusion determined using DWI and DCE-MRI parameters in NPC, to explore the possibility of noninvasively evaluating tumour perfusion using DWI in the future.

Materials and methods

Study population

This prospective study was reviewed by the ethics committee of our hospital, and all patients provided informed consent. From April 2012 to October 2013, we prospectively enrolled 38 patients with newly diagnosed NPC for MRI examinations. The maximum tumour area of each patient was determined from axial contrast-enhanced and unenhanced MR images.

Conventional MRI

MR imaging was performed using a 3-T MR system (Signa EXCITE HD; GE Healthcare, Milwaukee, WI, USA) with a 40 mT/m maximum gradient capability and employing a standard receive-only head and neck coil. We first obtained axial T1-weighted images [repetition time (TR)/echo time (TE), 600/23 ms] and axial T2-weighted turbo spin echo images with fat suppression [TR/TE, 5,200/137 ms; 4-mm section thickness, 1-mm intersection gap; number of excitations (NEX)=2] using a 512×288 imaging matrix.

IVIM DWI

The IVIM DWI sequence was performed before contrast-enhanced MRI. During the IVIM examination, 13 *b*-values (0, 10, 20, 30, 50, 80, 100, 150, 200, 300, 400, 600 and 800 s/mm^2) were applied using a single-shot spin echo echo- planar imaging sequence. The lookup table of gradient directions was modified accordingly to allow multiple *b*-value measurements in a single series. Parallel imaging was used with an acceleration factor of 2. A local shim box covering the region of the nasopharynx was applied to minimise susceptibility artefacts. Fourteen axial slices covering the nasopharynx were obtained with a 24-cm field of view, 4-mm slice thickness, 1-mm slice gap, 3,000 ms repetition time (TR), 58 ms echo time (TE), 128×128 matrix and 2 NEX. The nominal scan time was 3 min 45 s. Note that the signal-to-noise ratio (SNR) in the raw EPI images from the multiple b-value acquisitions was assessed as: SNR=0.655 S/SD$_{air}$, where S is the mean signal intensity in the ROI of NPC and SD$_{air}$ is the standard deviation in the background ROI in air.

IVIM-MRI analysis

Pure molecular diffusion (*D*), perfusion-related diffusion (*D**) and the perfusion fraction (*f*) were calculated using segmented biexponential analysis (Fig. 1). On the basis of IVIM theory, the relationship between the signal intensities and *b*-values can be expressed using the following equation:

$$S_b/S_0 = (1-f)exp(-b\cdot D) + f\cdot exp(-bD^*) \quad (1)$$

where *f* is the microvascular volume fraction representing the fraction of diffusion linked to microcirculation [16], *D* is a pure diffusion coefficient, and *D** represents perfusion-related incoherent microcirculation; S_0 and S_b are the signal intensities at *b*-values of 0 and 10, 20, 30, 50, 80, 100, 150, 200, 300,400, 600 or 800 s/mm^2, respectively. As *D** is much greater than *D* [9], the effects of *D** on signal decay at large *b*-values (>200 s/mm^2) can be ignored, and Eq. (1) can be simplified as follows:

$$S_b/S_0 = (1-f)exp(-b\cdot D) \quad (2)$$

All diffusion-weighted images were transferred to an Advantage Workstation using Functool software (version AW4.3, General Electric Medical Systems) for post-processing. All image analysis were performed with Multiple ADC (MADC) software in Functool and fitted on a pixel-by-pixel basis using the Levenberg-Marquardt algorithm, as previously described [17]. The three parameters were calculated consecutively, in which the *D* value was determined by using

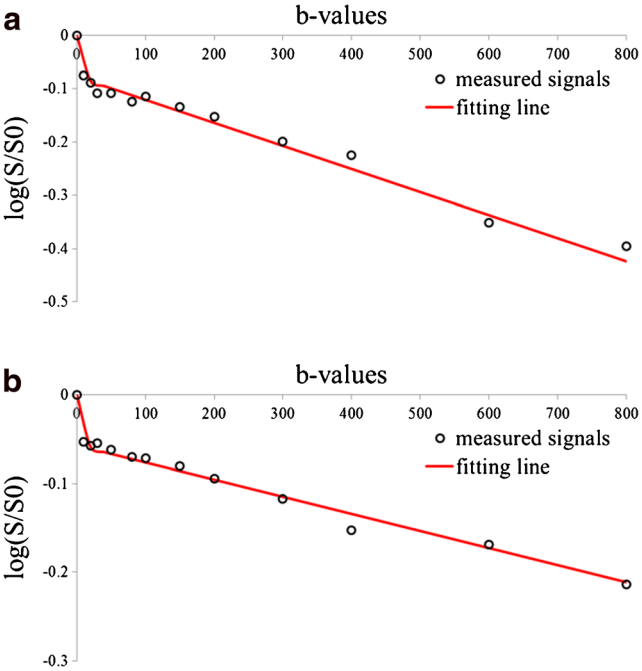

Fig. 1 IVIM diffusion decay curves shown for a 39-year-old male patient (**a**) and 46-year-old male patient (**b**) with newly diagnosed NPC. The same patients are also shown in Figs. 2 and 3. The *y*-axis shows the signal intensity (SI) ratio after application of the diffusion gradient to the baseline SI (plotted in log scale); the *x*-axis shows the *b*-values (the *b*-values 0, 10, 20, 30, 50, 80, 100, 150, 200, 300, 400, 600 and 800 s/mm^2 were used for sampling). The perfusion (or pseudo-diffusion) effect is observed as an early drop in the SI at *b*-values lower than 200 s/mm^2. The perfusion fraction (*f*) is the difference between the SI at *b*=0 s/mm^2 and the intercept of the biexponential fit for high *b*-values. D* (pseudo-diffusion coefficient) is the curvature of the initial curve, and D (true diffusion coefficient) was measured at *b*-values higher than 200 s/mm^2

Eq. (2). The *f* and *D** values were calculated by using a non-linear regression algorithm for all b values.

DCE-MRI

Axial T1-weighted images (TR/TE, 7.0/3.3 ms) were obtained using a three-dimensional (3D) spoiled gradient-recalled echo (SPGR) sequence [240×240 mm^2; field of view (FOV), 4-mm slice thickness; 15° flip angle; 256×160 matrix size]. Gadolinium (gadopentetate dimeglumine; Magnevist; Bayer HealthCare, Berlin, Germany) was intravenously injected using a power injector (Medrad, Pittsburgh, PA, USA) at 0.2 ml/kg body weight and 2 ml/s. Ten MR data acquisitions were obtained for each patient at an interval of 20 s (0-180 s). DCE-MRI parameters [maximum slope of increase (MSI), enhancement ratio (ER), enhancement amplitude (EA)] were calculated on an Advantage Workstation using Functool software (version AW4.3, General Electric Medical Systems). MSI and ER colour maps were generated using Functool software, and regions of interest (ROIs) were drawn around the tumours on both the MSI and ER colour-coded images. Analysis was performed on data averaged across the whole

Table 1 Distribution of IVIM and DCE-MRI parameters

	Reader 1 (n=27)	Reader 2 first session (n=27)	Reader 2 second session (n=27)	Total (n=81)	F	$P^{\dagger}$
MSI (%/s)	349.770±127.343	347.041±120.250	349.151±120.317	348.654±121.144	0.004	0.996
ER (%)	99.695±27.211	100.341±29.341	105.866±34.179	101.967±30.131	0.336	0.715
EA	640.878±149.010	636.259±145.667	641.270±154.965	639.469±148.062	0.009	0.991
D ($\times 10^{-3}$ mm^2/s)	0.755±0.203	0.747±0.200	0.762±0.200	0.754±0.198	0.036	0.965
f	0.167±0.037	0.170±0.033	0.165±0.035	0.167±0.0348	0.160	0.852
D* ($\times 10^{-3}$ mm^2/s)	138.026±42.643	143.780±37.437	149.938±34.682	143.914±38.228	0.650	0.525

Data are mean±standard deviation. † One-way ANOVA. F is the statistic

ROI. ER was defined as follows: $ER = (SI_{max} - SI_{pre})/SI_{pre}$, where SI_{max} was the signal intensity at maximal contrast enhancement, and SI_{pre} was the unenhanced ("precontrast") signal intensity. The MSI was calculated as $MSI = max[S(t_{i+1}) - S(t_i)]$, where max indicates maximum, S is signal intensity, t_i is the time point of the start of enhancement, and t_{i+1} is the time point of maximal enhancement. EA was measured directly from the time-signal intensity curves (TICs).

ROIs and reproducibility of measurements

A single slice of the axial DCE-MRI of the maximal area of each tumour was analysed in order to assess pairs of DCE-MRI and IVIM-MRI images from almost identical parts of each tumour. A ROI was manually placed on the tumour in each image to include as much of the tumour area as possible but exclude large vessels and visually large necrotic areas. Contrast-enhanced and unenhanced T1-weighted MR images were used as references to determine the tumour areas on the corresponding IVIM and DCE-MRI images. Twenty-one cases were measured in the primary tumours, and 6 cases were measured in metastatic retropharyngeal lymph nodes. Two investigators (Zheng-Gen Zhou, 15 years' experience in head and neck radiology, observer 1; Shui-Xing Zhang, 12 years of experience in head and neck radiology, observer 2) placed the ROIs and analysed all of the IVIM and DCE-MRI images independently. The tumours did not have a sufficiently large solid area for placing ROIs with a short-axis diameter greater than 10 mm were excluded (Analysis of tumours with small areas is often hampered by substantial edge artefacts). The data generated by the two observers was used to calculate interobserver reproducibility. To assess intraobserver reproducibility, observer 2 reevaluated all of the images, which were presented in a different order, 4 weeks after the first session.

Statistical analysis

Normality testing was performed using the Shapiro-Wilk test and homogeneity of variance testing using the Levene test. Numerical data are reported as the mean±standard deviation of all three sets of measurement. The intraclass correlation coefficient (ICC) and coefficient of variation (CV) were calculated to evaluate intra- and interobserver variability. We also analysed the level of agreement (both inter- and intraobserver) by plotting the differences between the two measurements against the averages of the two measurements, according to the method described by Bland and Altman (i.e. Bland-Altman plots) [18]. The differences between the three sets of data determined by the two observers (observer 2 had 2 sets) were assessed using one-way ANOVA. The mean values of the three sets of data were used for the correlation analysis. Spearman's rank correlation coefficient was calculated to measure the association between the IVIM and MRI-DCE parameters. All analyses (except Bland-Altman plots) were performed using SPSS version 13.0 for Windows (SPSS, Chicago, IL, USA). For all tests, two-tailed P-values<0.05 were considered statistically significant.

Results

Patients

Of the 38 patients with newly diagnosed NPC enrolled into this study, 11 (29 %) patients were excluded from the study. In eight patients, the tumours did not have a sufficiently large solid area for placing ROIs with a short-axis diameter greater than 10 mm; in three patients, image degradation was very

Fig. 2 DCE parameters for a 39-year-old male with NPC (same patient as Fig. 1a). (**a**) A ROI was drawn around the entire tumour area on the contrast-enhanced T1-weighted MR image; (**b**) MSI (maximum slope of increase) map showing MSI=387.89 %/s; (**c**) ER (enhancement ratio) map demonstrating ER=67.453 %; (**d**) TICs (time-signal intensity curves) showing EA (enhancement amplitude)=758.6. IVIM parameters for the same patient. (**e**) A ROI was drawn around entire tumour area to measure signal intensity on the DW image at b=0; (**f**) D (true diffusion coefficient) map showing D=0.998×10^{-3} mm^2/s; (**g**) f (perfusion fraction) map demonstrating f=0.163; (**h**) D* (pseudo-diffusion coefficient) map showing D*=235×10^{-3} mm^2/s

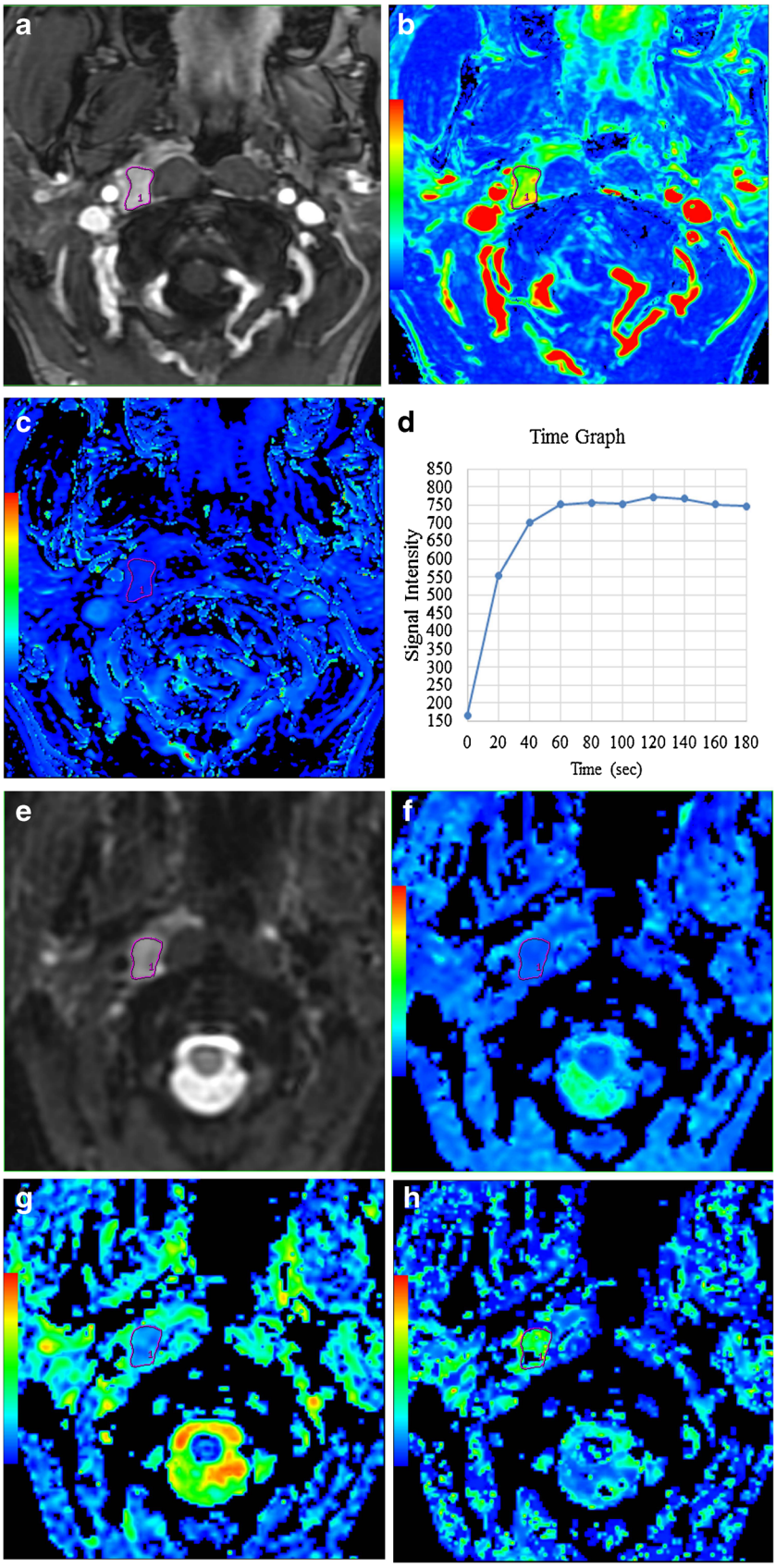
a
b
c
d
Time Graph
Signal Intensity
850
800
750
700
650
600
550
500
450
400
350
300
250
200
150
0 20 40 60 80 100 120 140 160 180
Time (sec)
e
f
g
h

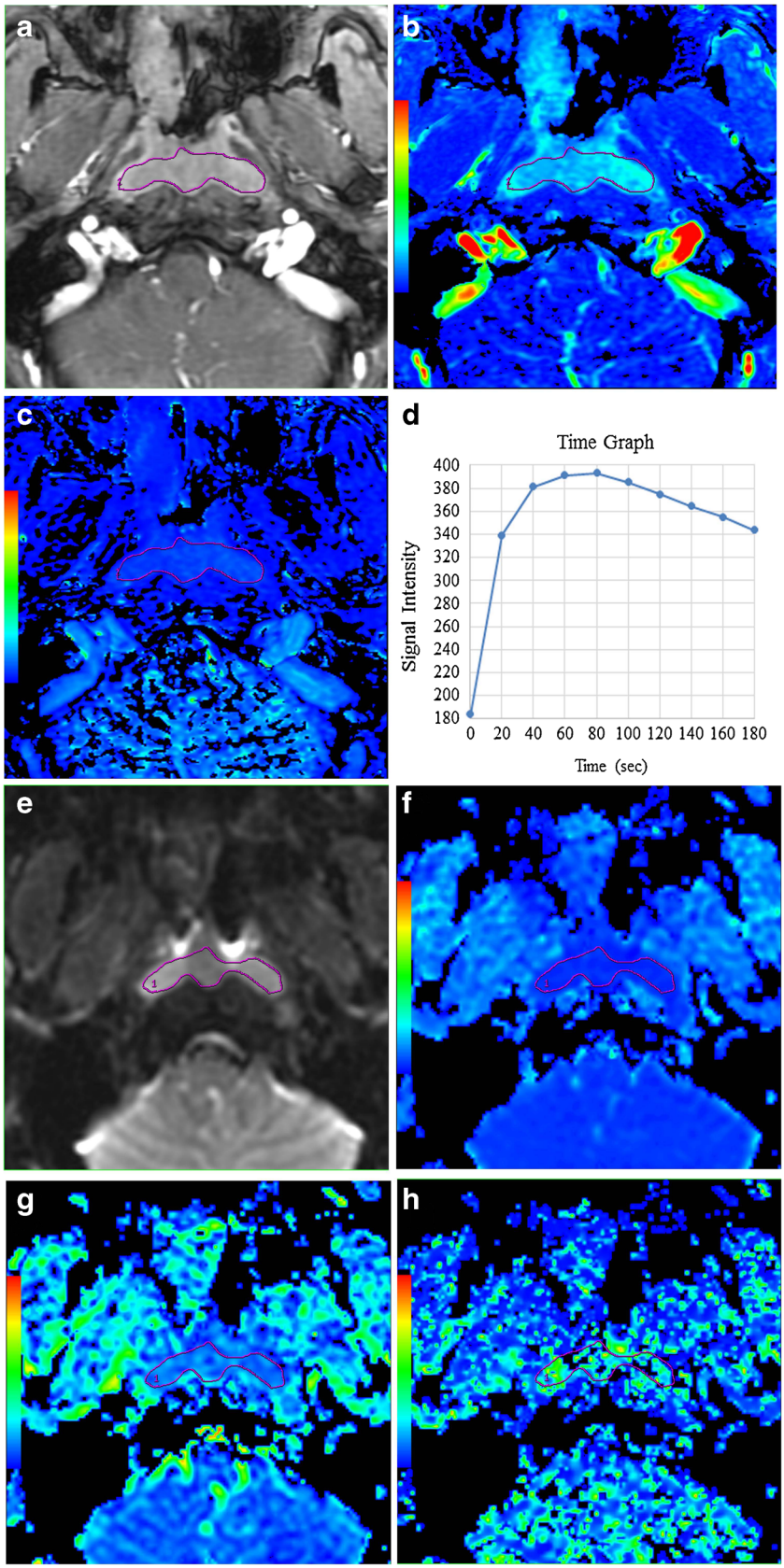
a
b
c
d
Time Graph
Signal Intensity
400
380
360
340
320
300
280
260
240
220
200
180
0 20 40 60 80 100 120 140 160 180
Time (sec)
e
f
g
h

◀ **Fig. 3** DCE parameters for a 46-year-old male with NPC (same patient as Fig. 1b). (**a**) A ROI was drawn around entire tumour area on the contrast-enhanced T1-weighted MR image; (**b**) MSI (maximum slope of increase) map showing MSI=155.42 %/s; (**c**) ER (enhancement ratio) map demonstrating ER=98.620 %; (**d**) TICs (time-signal intensity curves) showing EA (enhancement amplitude)=390.1. IVIM parameters for the same patient. (**e**) A ROI was drawn around entire tumour area to measure signal intensity on the DW image at b=0; (**f**) D (true diffusion coefficient) map showing $D=0.444\times10^{-3}$ mm^2/s; (**g**) f (perfusion fraction) map demonstrating f=0.123; (**h**) D* (pseudo-diffusion coefficient) map showing $D^*=175\times10^{-3}$ mm^2/s

severe. Thus, we studied 27 consecutive patients with NPC (17 males, 10 females; mean±standard deviation age, 49.4± 12.4 years, range: 27–65 years). The mean±standard deviation tumour size (determined by the maximum tumour areas on axial contrast-enhanced and unenhanced MR images) was 214.4±131.1 mm^2 (range, 79.6-481.3 mm^2).

DCE and IVIM parameters

Normality testing showed that all DCE (MSI, ER and EA) and IVIM (*D, f* and *D**) parameters had approximately normal distributions (all $P>0.05$), and the Levene test revealed that all the variances were homogeneous (all $P>0.05$). Table 1 summarises the mean and standard deviation values of the IVIM and DCE parameters. There was no significant difference between the three sets of DCE (MSI, ER and EA) and IVIM (*D, f* and *D**) parameters determined by observer 1 and 2 (P= 0.525-0.996). The IVIM diffusion decay curves are shown in Fig. 1. Representative examples of the MRI-DCE and IVIM images are shown in Figs. 2 and 3, illustrating the typical colour changes in the respective parameter maps. SNR was typically above 15 (range from 18.73 to 57.99) for all b-values.

Intra- and interobserver reproducibility

Intra- and interobserver reproducibility for measurement of the DCE (MSI, ER and EA) and IVIM (*D, f* and *D**) parameters are presented in Table 2. Excellent intra- and interobserver reproducibility was obtained for all DCE parameters (MSI, ER and EA) and the IVIM parameters *D* and *f*, with ICC values ranging from 0.955 to 0.997 and 0.945 to 0.988, respectively. Intra- and interobserver reproducibility for *D** was relatively good, with ICC values of 0.922 and 0.887, respectively. The intraobserver CV ranged from 4.420 % to 11.286 %, and the inter-observer CV ranged from 7.813 % to 14.162 %. Bland-Altman plots for the DCE parameters and IVIM parameters revealed small absolute intra- and interobserver (Fig. 4) variability, and the 95 % LoAs (limits of agreement) for the DCE and IVIM parameters are presented in Table 3.

Correlations between parameters of DCE and IVIM

The correlations between the DCE parameters (MSI, ER and EA) and IVIM perfusion-related parameters (*f* and *D**) were assessed using Spearman's r values and are presented in Table 4. The highest correlation was observed between *f* and EA (r=0.633, $P<0.001$; Fig. 5a). A strong correlation was also found between *f* and MSI (r=0.598, P=0.001; Fig. 5b). However, statistically significant correlation was not observed between *f* and ER (r=-0.162; P= 0.421) or between *D** and any DCE parameter including MSI (r=0.125; P= 0.536), ER (r=-0.226; P= 0.257) and EA (r=0.307; P= 0.119).

Discussion

According to IVIM theory [8], the use of a more sophisticated approach to describe the relationship between signal attenuation in tissues with increasing *b*-values would generate quantitative parameters that separately reflect tissue perfusion and tissue diffusivity. The behaviour of protons that display signal attenuation in DWI is termed IVIM. Using biexponential analysis, it is possible to derive IVIM parameters that quantitatively describe tissue perfusion (pseudo-diffusion coefficient, *D**), the perfusion fraction of tissues (*f*) and tissue water diffusivity (*D*) [8, 19, 20].

The *f* value measures the fractional volume of capillary blood flowing in each voxel. Direct correlations have been suggested between *f* and the extent of normal

Table 2 Intra- and interobserver reproducibility in the assessment of IVIM and DCE-MRI parameters

Parameter	Intraclass coefficient correlation (95 % CI)		Coefficient of variation (%)	
	Intraobserver	Interobserver	Intraobserver	Interobserver
MSI	0.996 (0.990-0.998)	0.988 (0.974-0.995)	4.420	7.813
ER	0.990 (0.979-0.996)	0.963 (0.920-0.983)	6.982	8.649
EA	0.997 (0.993-0.999)	0.985 (0.967-0.993)	4.834	7.978
D	0.991 (0.980-0.996)	0.977 (0.950-0.990)	5.275	8.306
f	0.955 (0.902-0.980)	0.945 (0.879-0.975)	8.099	10.646
*D**	0.922 (0.828-0.964)	0.887 (0.751-0.948)	11.286	14.162

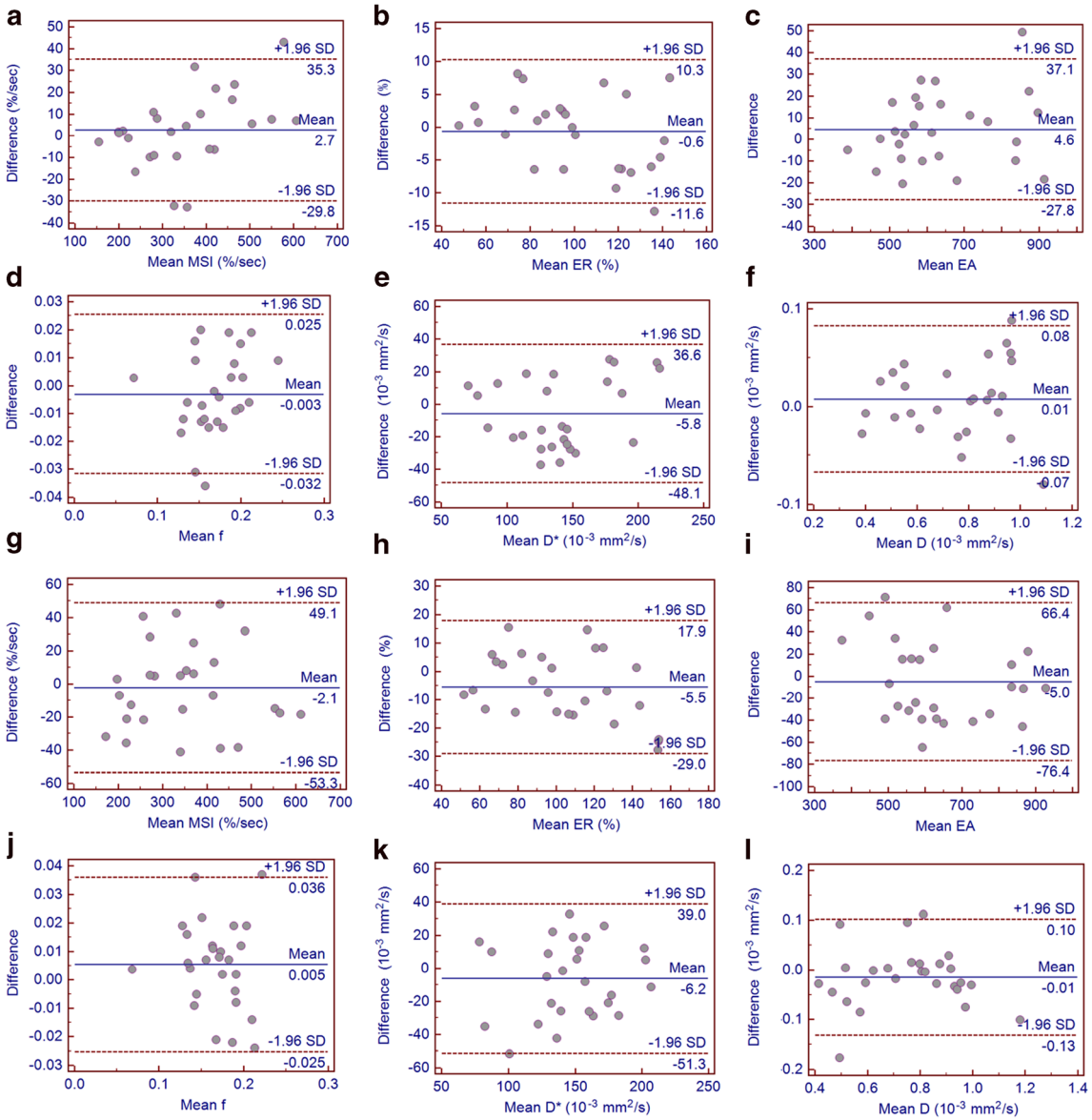

Fig. 4 Bland-Altman plots of intraobserver reproducibility for the DCE parameters MSI (**a**), ER (**b**) and EA (**c**), and IVIM parameters *f* (**d**), *D** (**e**) and *D* (**f**). Bland-Altman plots of interobserver reproducibility for the DCE parameters MSI (**g**), ER (**h**) and EA (**i**), and IVIM parameters *f* (**j**), *D** (**k**) and *D* (**l**)

angiogenesis with intact vessels in terms of basement membrane thickness and pericyte coverage; therefore, *f* may be an indicator of vascular permeability [10, 21]. *D**, which is determined as the signal intensity ratios of blood capillaries, is linked to perfusion, which in turn may be dependent on tumour microvessel attenuation. *D** was reported to be proportional to the mean capillary segment length and average blood velocity; thus, it is reflective of tumour vascularity [8]. Additionally, *f* and *D** are significantly correlated with the microvessel

Table 3 Intra- and interobserver variation in the assessment of IVIM and DCE-MRI parameters

	MSI (%/s)	ER (%)	EA	*f*	*D** ($\times 10^{-3}$ mm^2/s)	*D* ($\times 10^{-3}$ mm^2/s)
Intraobserver	−29.8-35.3	−11.6-10.3	−27.8-37.1	−0.032-0.025	−48.1-36.6	−0.07-0.08
Interobserver	−53.3-49.1	−29.0-17.9	−76.4-66.4	−0.025-0.036	−51.3-39.0	−0.13-0.10

Values are presented as 95 % limits of agreement (LoA; mean interdevice difference, spans of limits of agreement)

Table 4 Correlations between IVIM and DCE-MRI parameters in NPC

	f		*D**	
	r	*P*-value	*r*	*P*-value
MSI	0.598†	0.001	0.125	0.536
ER	−0.162	0.421	−0.226	0.257
EA	0.633†	<0.001	0.307	0.119

† Statistically significant ($P<0.05$), Spearman's rank correlation

density (MVD), which is commonly used as a surrogate marker of angiogenesis [22].

The time-signal intensity curve (TIC) profiles obtained by DCE-MRI can indicate tumour tissues in which biomarkers of angiogenesis are present: MSI correlates with the pericyte coverage index and expression of vascular endothelial growth factor receptor 2 (VEGFR-2), and EA correlates with expression of VEGFR-2 [23]. Both semiquantitative and quantitative DCE-MRI analysis may potentially help to characterise the neovasculature and permeability in NPC. The neovasculature of tumours in patients with higher T-category NPC exhibit increased permeability and perfusion; therefore, DCE-MRI may be helpful as an adjunct technique for evaluating NPC [4]. In this study we investigated the semiquantitative DCE-MRI parameters (MSI, ER and EA) in patients with NPC. The major limitation of this semiquantitative method is that it does not accurately and directly reflect the concentration of contrast agent in the tissue of interest, rather it captures the information from the signal intensity curves. However, Huang et al. [4] demonstrated the robustness of these semiquantitative methods to indirectly reflect tissue physiology in NPC compared to the quantitative method. Furthermore, the advantage of semiquantitative analysis is that it provides a more straightforward quantification of DCE-MR images that is directly related to the enhancement pattern of the tumour, which is feasible in routine clinical practice.

One important issue related to IVIM and DCE-MRI is reproducibility. Patel et al. [24] reported good to excellent reproducibility for *D* and *f*, especially when using a navigator-triggered acquisition, in the evaluation of liver cirrhosis (CV<6 % for *D*; < 12 % for *f*) and found that *D** had the poorest reproducibility (CV of 14.6 % for navigator-triggered and free breathing acquisitions). In a recent study [7], the ranges of the interobserver agreement values for *D, f* and *D** determined by IVIM in the breast were excellent (*D* and *f*) to relatively good (*D**). Furthermore, the distribution of the IVIM imaging parameters (*D, f* and *D**) obtained in this study is almost similar to those of the study by Lai et al. [14, 15] in NPC using a 3.0-T MRI (Philips Healthcare).

The number of *b*-values used for extracting perfusion-sensitive information during DWI varies between studies and ranges from four to more than ten. A larger number of *b*-values provides more data support for the estimates and, in particular, enables parameter uncertainties to be evaluated. The accuracy of estimating *D** improved with sampling (i.e., as the number of *b*-values increased) in the 0–200 s/mm^2 range [16, 24]. Using an 11 *b*-value DWI sequence, Guiu et al. [25] applied seven *b*-values (0, 5, 15, 25, 35, 50, 100 s/mm^2) to model this first part of the biexponential decay encompassing both *D* and *D**. A 13 *b*-value DWI sequence was used in this study, of which 9 *b*-values were applied to model this part of the biexponential curve. Susceptibility artefacts increase with the use of higher *b*-values, typically around 1,000 s/mm^2. Furthermore, the poor signal-to noise ratio (SNR) obtained at higher *b*-values decreases the accuracy of IVIM calculations. Consequently, we tried to minimise this effect by setting the maximum *b*-value to 800 s/mm^2. As a result, we obtained excellent to relatively good intra- and interobserver reproducibility for the IVIM parameters, and the Bland-Altman plots for the IVIM parameters also confirmed small absolute intra- and interobserver variations.

Regarding the reproducibility of measuring DCE-MRI parameters, Miyazaki et al. [26] recently reported excellent reproducibility when measuring the hepatic perfusion index (a semiquantitative perfusion parameter) in patients treated with an antiangiogenic compound. The intra- and interobserver reproducibility of measuring the DCE-MRI parameters in our study was excellent to good.

Of note, in the present study, reproducibility referred to observer. The test-retest reproducibility was not addressed because it was not ethical to assign MRI examination twice on the same patients.

Although no publications on the relationship between SNR and the accuracy of DWI estimation have been reported, it has been shown that, for DWI estimation, an SNR of 10-15 of the raw images allows accurate ADCs for DWI acquisition [27, 28]. The use of local shim, parallel imaging and improved SNR at 3.0 T yielded high-quality IVIM DW imaging in our study. Given the high SNRs (>15 for all b-values) in the current study, the quantitation of *D*, *D**, and *f* should not be affected substantially by the SNR variations between different b-values.

The relationship between perfusion parameters measured using IVIM versus those measured with DCE-MRI is unclear. In theory, there should be close agreement between perfusion parameters quantified by DWI and other techniques [20]. Le Bihan and Turner reasoned that, even with the use of freely diffusible tracers, delivery of the tracer to the tissues is still dependent on intravascular flow; thus, it is highly likely that there is a relationship between tissue perfusion measured using DWI and tracer kinetic methods [10]. In a contradictive opinion article, Henkelman [29] suggested that IVIM does not measure tissue perfusion in the same manner as DCE-MRI does, as IVIM is more sensitive to blood volume transit through a voxel. Data corroborating or contradicting these

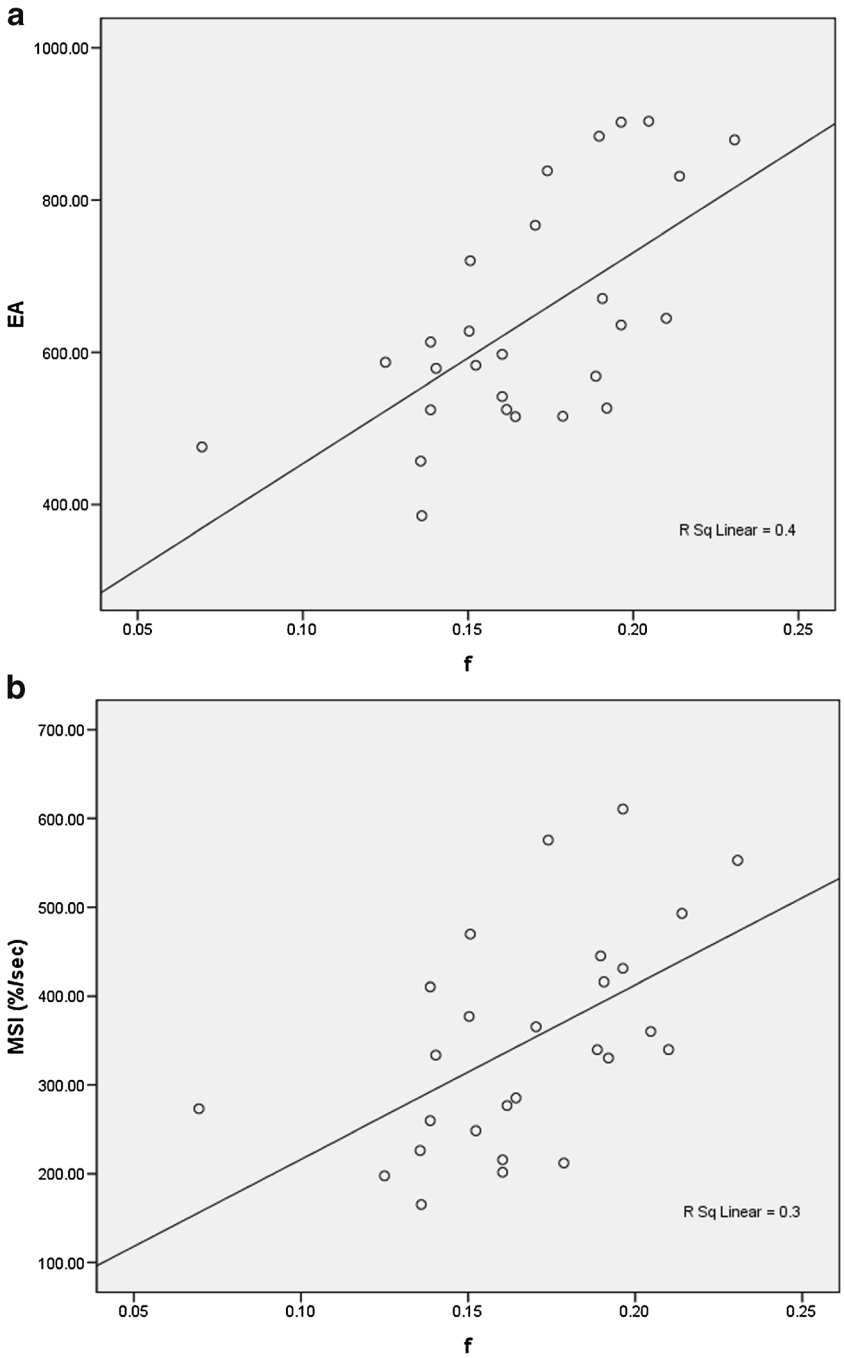

Fig. 5 **a** Correlation between EA and *f*. EA correlated significantly with *f* (r=0.633, P<0.001). **b** Correlation between MSI and *f*. MSI correlated significantly with *f* (r=0.598, P=0.001)

opinions are sparse, even in neuroimaging. In the published literature, IVIM-derived perfusion indexes have been reported to correlate with perfusion parameters derived using other techniques. One study [30] of the brains of 28 volunteers compared IVIM-based analysis with assessment of relative cerebral blood flow and relative cerebral blood volume using dynamic susceptibility contrast enhancement imaging, and found that *f* correlated well with the relative cerebral blood volume, and *D** correlated with cerebral relative blood flow. Another study of the brains of seven patients showed that *f* correlated well with the dynamic susceptibility contrast parameter cerebral blood volume [11]. However, Patel et al. [24] suggested that IVIM liver perfusion measurements were not equivalent and did not correlate with DCE-MRI perfusion parameters.

In the present study, *f* correlated significantly with EA and MSI, while *D** had no significant correlation with any DCE parameter. Unexpectedly, *D** did not correlate with the IVIM perfusion-related parameters, in contradiction to IVIM theory. Of the IVIM parameters, the reproducibility of measuring *D** was relatively poor; the values for *f* lay within a relatively narrow range, whereas the values of D* were more variable.

Furthermore, *D** may more accurately reflect the true dynamics of flow than DCE, in which flow is artefactually reduced because of contrast leakage [11]. Of course, the precise reasons leading to these results need further research; for example, in a larger cohort of patients NPC and including measurement of biomarkers of angiogenesis.

The IVIM method has a number of theoretical advantages compared to the more commonly used MRI perfusion method DSC. IVIM may have a potentially higher resolution and is more sensitive to incoherent flow arising in small vessels, while the DSC signal is polluted by signal from large arteries and veins [31]. Furthermore, IVIM can be performed without the administration of exogenous contrast medium, making it a safer and more convenient evaluation method for patients, especially individuals with renal insufficiency.

This study has several limitations. Two major limitations are the relatively small patient cohort and the absence of the measurement of angiogenesis biomarkers. A similar analysis on a larger cohort of patients with NPC accompanied by measurement of angiogenesis biomarkers to compare IVIM perfusion-related and DCE parameters may provide more reliable results. Another major limitation of this study is the constraint on tumour size in the DCE and IVIM analyses. As stated in the Materials and methods section, we excluded tumours that were too small from the analysis. Furthermore, IVIM DWI was unsuccessful in approximately 8 % of the patients in our study because of severe image degradation resulting from magnetic field inhomogeneities at the air-bone and air-soft tissue interfaces around the skull base and motion artefacts caused by physiological activity, similarly to a previous DWI study of the nasopharynx [32].

Conclusion

In conclusion, we present our initial clinical experience with IVIM in NPC, which demonstrates that IVIM can produce clinically relevant high-resolution perfusion maps. We found that the IVIM parameter *f* correlates significantly with the DCE parameters EA and MSI. As it measures perfusion directly, locally and without the need for contrast agent, the use of IVIM to assess tumour perfusion should be more widely investigated in large laboratory and clinical studies in the future.

Acknowledgments This work was supported by grants from the National Natural Science Foundation of China (nos. 81271654, 81271569 and 81171329) and Science and Technology Support Program of Guangzhou, China (2010J-E481). We gratefully acknowledge the assistance of Zhong-Ping Zhang (MD, from Applied Science Lab, GE Healthcare, Guangzhou, Guangdong Prov., P. R. China) for support with IVIM methodology and for linguistic editing.

The scientific guarantor of this publication is Chang-Hong Liang. The authors of this manuscript declare relationships with the following companies: GE Healthcare. No complex statistical methods were necessary for this paper. Institutional Review Board approval was obtained. Written informed consent was obtained from all subjects (patients) in this study. Methodology: Prospective, diagnostic or prognostic study, performed at one institution.

References

1. Parkin DM, Bray F, Ferlay J, Pisani P (2005) Global cancer statistics, 2002. CA Cancer J Clin 55:74–108
2. Fu Y-S, Wenig BM, Abemayor E, Wenig B (2001) Head and neck pathology with clinical correlations. Philadelphia (Pa) 7:602
3. Jin G, Su D, Liu L, Zhu X, Xie D, Zhao W (2011) The accuracy of computed tomographic perfusion in detecting recurrent nasopharyngeal carcinoma after radiation therapy. J Comput Assist Tomogr 35: 26–30
4. Huang B, Wong CS, Whitcher B et al (2013) Dynamic contrast-enhanced magnetic resonance imaging for characterising nasopharyngeal carcinoma: comparison of semiquantitative and quantitative parameters and correlation with tumour stage. Eur Radiol 23:1495–1502
5. Semiz Oysu A, Ayanoglu E, Kodalli N, Oysu C, Uneri C, Erzen C (2005) Dynamic contrast-enhanced MRI in the differentiation of posttreatment fibrosis from recurrent carcinoma of the head and neck. Clin Imaging 29:307–312
6. Lee FK, King AD, Ma BB, Yeung DK (2012) Dynamic contrast enhancement magnetic resonance imaging (DCE-MRI) for differential diagnosis in head and neck cancers. Eur J Radiol 81:784–788
7. Liu C, Liang C, Liu Z, Zhang S, Huang B (2013) Intravoxel incoherent motion (IVIM) in evaluation of breast lesions: comparison with conventional DWI. Eur J Radiol 82:e782–e789
8. Le Bihan D, Breton E, Lallemand D, Aubin ML, Vignaud J, Laval-Jeantet M (1988) Separation of diffusion and perfusion in intravoxel incoherent motion MR imaging. Radiology 168:497–505
9. Le Bihan D, Turner R, MacFall JR (1989) Effects of intravoxel incoherent motions (IVIM) in steady-state free precession (SSFP) imaging: application to molecular diffusion imaging. Magn Reson Med 10:324–337
10. Le Bihan D, Turner R (1992) The capillary network: a link between IVIM and classical perfusion. Magn Reson Med 27:171–178
11. Federau C, O'Brien K, Meuli R, Hagmann P, Maeder P (2013) Measuring brain perfusion with intravoxel incoherent motion (IVIM): initial clinical experience. J Magn Reson Imaging. doi:10.1002/jmri.24195
12. Sumi M, Van Cauteren M, Sumi T, Obara M, Ichikawa Y, Nakamura T (2012) Salivary gland tumors: use of intravoxel incoherent motion MR imaging for assessment of diffusion and perfusion for the differentiation of benign from malignant tumors. Radiology 263:770–777
13. Sumi M, Nakamura T (2013) Head and neck tumours: combined MRI assessment based on IVIM and TIC analyses for the differentiation of tumors of different histological types. Eur Radiol. doi:10.1007/s00330-013-3002-z
14. Lai V, Li X, Lee VH, Lam KO, Chan Q, Khong PL (2013) Intravoxel incoherent motion MR imaging: comparison of diffusion and perfusion characteristics between nasopharyngeal carcinoma and post-chemoradiation fibrosis. Eur Radiol. doi:10.1007/s00330-013-2889-8
15. Lai V, Li X, Lee VH et al (2013) Nasopharyngeal carcinoma: comparison of diffusion and perfusion characteristics between different tumour stages using intravoxel incoherent motion MR imaging. Eur Radiol. doi:10.1007/s00330-013-2995-7
16. Luciani A, Vignaud A, Cavet M et al (2008) Liver cirrhosis: intravoxel incoherent motion MR imaging–pilot study. Radiology 249:891–899

17. Pang Y, Turkbey B, Bernardo M et al (2013) Intravoxel incoherent motion MR imaging for prostate cancer: an evaluation of perfusion fraction and diffusion coefficient derived from different b-value combinations. Magn Reson Med 69:553–562
18. Bland JM, Altman DG (1986) Statistical methods for assessing agreement between two methods of clinical measurement. Lancet 1:307–310
19. Zhang JL, Sigmund EE, Chandarana H et al (2010) Variability of renal apparent diffusion coefficients: limitations of the monoexponential model for diffusion quantification. Radiology 254:783–792
20. Koh DM, Collins DJ, Orton MR (2011) Intravoxel incoherent motion in body diffusion-weighted MRI: reality and challenges. AJR Am J Roentgenol 196:1351–1361
21. Lewin M, Fartoux L, Vignaud A, Arrive L, Menu Y, Rosmorduc O (2011) The diffusion-weighted imaging perfusion fraction f is a potential marker of sorafenib treatment in advanced hepatocellular carcinoma: a pilot study. Eur Radiol 21:281–290
22. Lee HJ, Rha SY, Chung YE et al (2013) Tumor perfusion-related parameter of diffusion-weighted magnetic resonance imaging: correlation with histological microvessel density. Magn Reson Med. doi: 10.1002/mrm.24810
23. Thomassin-Naggara I, Bazot M, Darai E, Callard P, Thomassin J, Cuenod CA (2008) Epithelial ovarian tumors: value of dynamic contrast-enhanced MR imaging and correlation with tumor angiogenesis. Radiology 248:148–159
24. Patel J, Sigmund EE, Rusinek H, Oei M, Babb JS, Taouli B (2010) Diagnosis of cirrhosis with intravoxel incoherent motion diffusion MRI and dynamic contrast-enhanced MRI alone and in combination: preliminary experience. J Magn Reson Imaging 31:589–600
25. Guiu B, Petit JM, Capitan V et al (2012) Intravoxel incoherent motion diffusion-weighted imaging in nonalcoholic fatty liver disease: a 3.0-T MR study. Radiology 265:96–103
26. Miyazaki K, Collins DJ, Walker-Samuel S et al (2008) Quantitative mapping of hepatic perfusion index using MR imaging: a potential reproducible tool for assessing tumour response to treatment with the antiangiogenic compound BIBF 1120, a potent triple angiokinase inhibitor. Eur Radiol 18:1414–1421
27. Pierpaoli C, Basser PJ (1996) Toward a quantitative assessment of diffusion anisotropy. Magn Reson Med 36:893–906
28. Jones DK (2004) The effect of gradient sampling schemes on measures derived from diffusion tensor MRI: a Monte Carlo study. Magn Reson Med 51:807–815
29. Henkelman RM (1990) Does IVIM measure classical perfusion? Magn Reson Med 16:470–475
30. Wirestam R, Borg M, Brockstedt S, Lindgren A, Holtas S, Stahlberg F (2001) Perfusion-related parameters in intravoxel incoherent motion MR imaging compared with CBV and CBF measured by dynamic susceptibility-contrast MR technique. Acta Radiol 42:123–128
31. Edelman RR, Mattle HP, Atkinson DJ et al (1990) Cerebral blood flow: assessment with dynamic contrast-enhanced T2*-weighted MR imaging at 1.5 T. Radiology 176:211–220
32. King AD, Ahuja AT, Yeung DK et al (2007) Malignant cervical lymphadenopathy: diagnostic accuracy of diffusion-weighted MR imaging. Radiology 245:806–813